Phase transitions of pyrogenic silica suspensions: A comparison to model laponite

Uwe Kätzel, Thomas Richter, and Michael Stintz*
Research Group Mechanical Process Engineering, Institute of Process Engineering and Environmental Technology, TU Dresden, D-01062 Dresden, Germany

Herbert Barthel and Torsten Gottschalk-Gaudig
Wacker-Chemie AG, Werk Burghausen, Johannes-Hess-Strasse 24, D-84480 Burghausen, Germany
(Received 20 September 2006; revised manuscript received 18 June 2007; published 18 September 2007)

Pyrogenic silica is often used as a thickening agent in paints, pastes, adhesives, or resins. Other applications include, e.g., abrasives in chemical mechanical planarization in the microelectronics industry. In all these applications it is essential to control the state of dispersion. Sometimes, phase transitions from the liquid to the solid state are required while in other cases they have to be completely avoided for the whole shelf life. The nature and influencing parameters of the fluid-solid transition for pyrogenic silica have not been investigated so far. Most investigations deal with the phase transitions of small clay particles such as laponite. Here, we dedicate our interest to the behavior of pyrogenic silica suspensions with varying specific surface area and ionic background concentration. To get an impression of the phase transition behavior we compare our results to model laponite suspensions. We apply dynamic light scattering measurements in the backscattering regime to minimize multiple scattering contributions from concentrated pyrogenic silica suspensions. Further on we exert a decomposition of the measured autocorrelation functions into an ergodic and nonergodic contribution. The analysis of the ergodic spectrum yields two different gelation kinetics for both systems, laponite and pyrogenic silica. For laponite these are in accordance with earlier investigations. The kinetics depend on the ionic background and the solids content of the suspensions. Additionally, we used dynamic extinction spectroscopy to follow the phase transitions of pyrogenic silica on a macroscale.

DOI: 10.1103/PhysRevE.76.031402 PACS number(s): 82.70.Dd, 83.80.Hj, 82.70.Gg, 05.70.Fh

I. INTRODUCTION

Recently, the interest in colloidal particles in science and industry has increased enormously. Colloidal particles are part of adhesives, paints, or abrasives used in the chemical, automotive, or microelectronic industry. They provide specific properties for the end products such as gloss, smoothness, planarity, hardness, or viscosity. These properties are caused by the large surface area of the particles compared to their volume and mass. In fluids the decreasing influence of body forces such as gravitation leads to diffusion dominated characteristics. Surface potentials such as van der Waals attraction and electrostatic repulsion become more important. The superposition of these different energies as described by the DLVO (Derjaguin, Landau, Verwey, and Overbeck) theory [1] involves a total interaction potential between two opposing particles at a given distance, either attracting or repulsing.

The interplay of these forces can under certain circumstances lead to a fluid-solid phase transition of a colloidal suspension. Within the scope of this investigation we only consider reversible phase transitions. Such phase transition processes are known for different colloidal suspensions though they are not fully understood, yet. They depend on time, the concentration of the colloidal particles, the temperature, and the magnitude of the interparticle forces. Sometimes these phase transitions are wanted, e.g., for cosmetic or medical applications. In other cases, they are unwanted as they affect the stability of the end product, e.g., in paints or abrasives. This indicates that the phase transition time, i.e., the time required for a complete solidification, is one of the most important process parameters in industrial applications. It should be controllably short for wanted phase transitions and very long if a transition has to be avoided. Analytical techniques, mostly based on dynamic light scattering, have been developed to determine the phase transition time and the transition kinetics of colloidal suspensions [2,3]. The transition time can be influenced by the particle concentration [2], the salinity [4], and the *p*H of the suspension [5].

According to Tanaka *et al.* [6] the suspension structures evolving during a phase transition can be divided into colloidal repulsive Wigner glasses, attractive glasses, and attractive gels. Wigner glasses are formed when repulsion between the particles leads to a confinement in cages if the volume fraction φ of the suspension is sufficiently high. An accepted value for the glass transition concentration of hard sphere suspensions is $\varphi_g=0.58$ [7,8].

If the contribution of the repulsive force is of the same order of magnitude as that of the attractive force the final structure is called an attractive glass. Experiments [3,9,10] and simulations [11,12] support this model. At low concentrations clusters of finite size at an energetic minimum level are formed by attractive forces [12]. At high cluster volume fractions repulsive interaction forces can lead to a complete phase transition due to excluded-volume interactions.

In the case of dominating attractive forces the particles agglomerate to clusters which finally interconnect to form the fractal network of a gel. Thereby, the maximum cluster

*Electronic address: Michael.Stintz@tu-dresden.de; URL: http://www.mvt-tu-dresden.de

size is limited depending on the strength of the interparticle forces (strong forces yield many small clusters) [13,14], the density difference between fluid and solid [15], and thermal differences [16]. Sandkühler *et al.* [17], who described the gelation process as a two step scenario of an agglomeration step followed by an interconnection step, realized that the second step appears much faster for low volume fractions.

It should be noticed that the model of the three different structures is a hypothesis and is still under controversial debate. Especially, the glassy state gives rise to doubts for specific materials (see, e.g., Ref. [4]).

This paper aims to extend the understanding of phase transitions of pyrogenic silica depending on the ionic strength and the particle specific surface area. The size of the silica aggregates and the solid concentration at which phase transitions occur correspond to strongly scattering samples. Therefore, classical light scattering techniques as frequently used in earlier studies cannot be applied here. We use dynamic light scattering in the backscattering regime instead. As there are no data available with model systems in this regime, we first compare the results of the transition kinetics to laponite suspensions, which is widely accepted as a model system for those processes [2–4,6,18–21]. Section II describes the influence of the ion concentration on the system's resulting interparticle force and the theoretical background of dynamic light scattering, which was used for the experimental investigations. Additionally, data interpretation approaches for phase transitions will be presented. Subsequently, in Sec. III, an overview of the properties of both investigated systems as well as the sample preparation procedures are given. Further on, the utilized measurement instruments are explained. In Sec. IV, the experimental results of phase transitions of laponite and pyrogenic silica suspensions are presented and the resulting kinetics are compared. Section V gives a short conclusion and an outlook on further investigations.

II. THEORETICAL

A. Particle interactions

In aqueous systems a partial dissociation of surface groups such as OH groups leaves a charge on the particle's surface. This can be influenced by the *p*H value [5,22]. The dissolved ions in the suspension medium form a layer of counterions attached to the surface (Stern layer). A "loose" diffusive layer, caused by a decreasing surface potential and the Brownian motion of the ions, is adjacent to the Stern layer resulting in charge neutrality of the system. Both layers are often referred to as dielectric double layer. The overlap of the double layers of two particles leads to an increase in concentration of dissolved ions between the two particles, thus inducing an osmotic pressure that drives the particles apart. The formation of the dielectric double layer is therefore the main reason for colloidal stability in aqueous systems. The extension of the diffusive layer is scaled by the reciprocal Debye-Hückel parameter

$$\frac{1}{\kappa} = \left(\frac{\epsilon_0 \epsilon_r k_B T}{2e^2 N_A I_S} \right)^{1/2} \tag{1}$$

with $\epsilon_0 \epsilon_r$ as the product of the relative and the absolute permittivity, the Boltzmann constant k_B, the absolute temperature T, the elementary charge e, the Avogadro constant N_A, and the ionic strength I_S, which depends on the concentration of dissolved ions and their charge. By changing the temperature and the amount of dissolved ions, the thickness of the diffusive layer can be changed. While an increase of T leads to an increase of the thickness, an increase of I_S compresses the dielectric double layer. Thus, an increase of the ion concentration leads to a screening of the repulsive part of the interaction potential so that the mostly unchanged attractive forces may begin to dominate.

B. Dynamic light scattering

Dynamic light scattering (DLS) [23,24] has been used for the investigation of phase transition processes [2–4,7–9,15,16,18,19,25] in numerous publications since the nonintrusive observation of the motion of submicron particles is possible. The detected scattered light intensity of a DLS measurement is correlated and normalized as

$$g_2(\tau) = \frac{\langle I(t) I(t+\tau) \rangle}{\langle I(t) \rangle^2} \tag{2}$$

which is called the normalized autocorrelation function (ACF), with I as the scattered light intensity (commonly measured as the number of photons that are registered at the detector per unit time), t the waiting time, and τ the decay time. The angular brackets denote a temporal average. To receive information about the diffusive properties of the dispersed particles, their mean square displacement $\langle \triangle r^2 \rangle$ has to be known. According to the ergodic hypothesis of Boltzmann [26] in the case of ergodic systems the temporal average equals the spatial average. That is why for the ACF a temporal average of the scattering intensities is used instead. For nonergodic systems, the analysis of the ACF to obtain information on the diffusive properties of the system under investigation may lead to erroneous results.

Kroon *et al.* [2] discussed the separation of the measured scattered intensity into a fluctuating (I_f) part that only considers ergodic contributions to the scattered light intensity and a static (I_c) part

$$\langle I(t) \rangle = \langle I_f(t) \rangle + I_c. \tag{3}$$

Figure 1 shows an example of the development of I_f and I_c during a phase transition. In a system with free diffusion I_c is zero. It is defined as

$$I_c = \sqrt{2\langle I(t) \rangle^2 - \langle I(t)^2 \rangle}. \tag{4}$$

The correlation function obtained only for the fluctuating part of the scattered light intensities [correlation of the fluctuating field (CFF)] is then independent of nonergodic contributions [2]:

$$h(\tau) = 1 + \frac{\langle I(t) \rangle}{\langle I_f(t) \rangle} \{ \sqrt{g_2(\tau) - g_2(0) + 1} - 1 \}. \tag{5}$$

To calculate the CFF from the measured ACF a substitution as shown in the Appendix is performed to receive

$$h(\tau) = 1 + (1 - \sqrt{2 - g_2(0)})^{-1} \{ \sqrt{g_2(\tau) - g_2(0) + 1} - 1 \}. \tag{6}$$

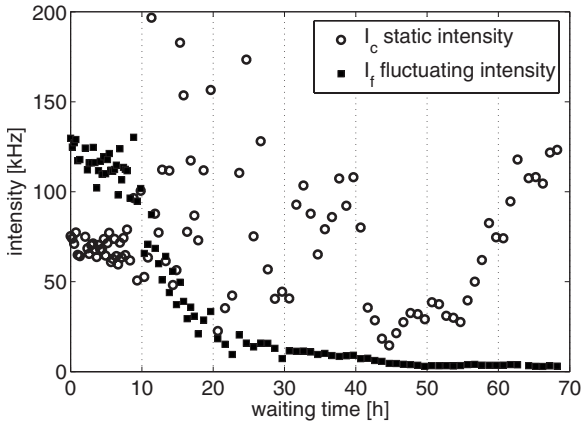

FIG. 1. Development of the fluctuating and static part of the scattered light intensities; sample: pyrogenic silica with $S_m = 100\ m^2/g$, 10.8 wt. %, $C_S = 0.1$ M.

A suspension that undergoes a phase transition shows a stretching of the long-time tail of the measured ACF from exponential to power-law behavior with increasing waiting time (see, e.g., Fig. 3). At the transition point from ergodic to nonergodic state the intercept value starts to vary. This is due to decorrelations from frozen-in particles as well as due to multiple scattering effects of growing clusters in gels. Concurrently nonzero long-time plateaus can occur that are designated as Debye-Waller factor [2]. This corresponds to strongly varying nonzero values of I_c depending on the position of the experiment in the cell. Abou *et al.* [25] characterize the measured ACF data by the combination of an exponential decay and a stretched exponential

$$g_2(\tau) - 1 = b\{a \exp(-\tau/\tau_1) + (1-a)\exp[-(\tau/\tau_2)^{\beta}]\}^2. \tag{7}$$

This provides better fits to the data than the often used single stretched exponential [2,18]. Equation (7) allows for a physical interpretation, as freely diffusing portions (rotational and translational) always remain during the phase transition.

Using only the fluctuating part of the correlation function an analog to Eq. (7) can be found:

$$h(\tau) = a \exp(-\tau/\tau_1) + (1-a)\exp[-(\tau/\tau_2)^{\beta}]. \tag{8}$$

Note that by decomposing the ACF to the CFF already a transformation of the second-order correlation to first order has been conducted. In principle the use of Eq. (8) for data interpretation seems to be quite obvious because the ergodic hypothesis is never violated by decomposing the ACF. This in turn is a prerequisite for reliable data analysis in dynamic light scattering.

If the stretched exponential is considered to be caused by a distribution of decay times the mean decay time can be obtained by [3]

$$\tau_{\text{mean}} = \tau_2 \frac{1}{\beta} \Gamma\left(\frac{1}{\beta}\right), \tag{9}$$

where $\Gamma(1/\beta)$ is the Euler-gamma function. The increase of the mean relaxation time diverges with the waiting time and can be fitted with

TABLE I. Survey of the prepared samples of laponite suspensions.

Mass fraction [wt. %]	Ionic strength [M] (NaCl)
2.82	0
2.24	0
1.96	0
1.29	0
2.29	4×10^{-4}
1.90	4×10^{-4}
1.00	5×10^{-3}

$$\tau_{\text{mean}} = \tau_0 \exp\left(B \frac{t}{t_{\text{PT}} - t}\right) \tag{10}$$

to obtain a phase-transition time t_{PT}. Further t is the waiting time and B is a constant.

III. EXPERIMENTAL

A. Materials and preparation

1. Laponite

Laponite RD or XLG (which is a specially purified type of laponite RD) are widely used materials to investigate phase transition processes in colloidal suspensions [2,3,6,20,25]. According to some authors [6,25] synthetic clay shows different phase transitions in dependence of the suspensions' ionic strength and solids content. Bonn *et al.* [27] published results that underline the glasslike character of pure laponite suspensions at a solids concentration of 3.5 wt. % without additional ions. Ruzicka *et al.* [3] showed that even for very low solids contents (up to 0.3 wt. %) phase transitions occur, the phase transition then lasts for months. However, the nature of the phase transitions is still under debate; e.g., Mongondry *et al.* [4] suppose that a glass state is not achieved for laponite suspensions.

The disc-shaped particles have a diameter of about 25 nm and a thickness of 1 nm [2]. In deionized water (18 M Ω/cm), the faces of the discs are strongly negatively charged, while the rims are positive. The high charge density of the faces results in long-ranged repulsive and short-ranged attractive forces. A screening of the repulsive forces via added ions facilitates aggregation [20]; however, aggregation should also be present at low ionic strengths [4]. Because of this specific charge behavior laponite particles are considered capable of forming different solid structures [3,6].

Suspensions with different laponite XLG concentrations and varying amounts of added sodium chloride were prepared. An overview of the samples is given in Table I. The required mass of laponite powder was weighed and added to a solution of deionized water and sodium chloride if necessary. After stirring for 30 min, the sample was treated in an ultrasonic bath (50 W) for 10 min. This routine was carried out twice. The suspension was finally filtered through a 0.4 μm membrane. This removes remaining agglomerates of

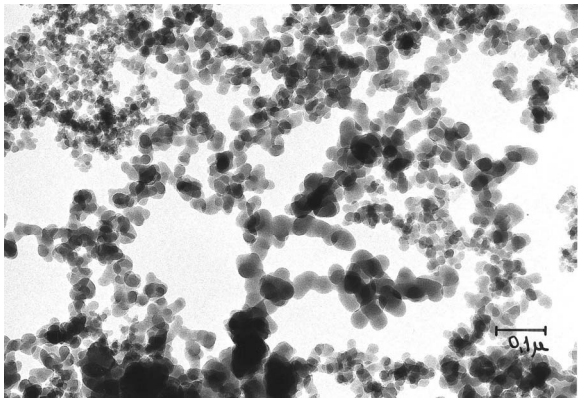

FIG. 2. TEM image of pyrogenic silica with a specific surface area of 150 m^2/g.

laponite that could otherwise hamper the identification of a certain phase transition process [28]. The procedure can cause a loss of laponite particles especially at higher weight fractions. Therefore, the exact mass fraction was afterwards determined via a halogen moisture balance. The resulting samples were colorless with a *p*H of about 10. All these steps were carried out in ambient atmosphere. It is known for laponite suspensions that a long-term contact with CO_2 can cause a release of magnesium ions from the particles that increases the ionic strength and speed up the phase transition process [29]. Therefore, after preparation the samples were filled in polycarbonate cuvettes and sealed with a gas-proof coverage. The remaining gas volume in the cuvette was minimal.

2. Pyrogenic silica

Pyrogenic silica is synthesized by high-temperature hydrolysis of tetrachlorosilane in a hydrogen/oxygen flame at temperatures of about 1750–2000 °C [30]. At these high temperatures spherical primary particles (5–30 nm) are formed, which sinter to fractal aggregates. Changing the process parameters (flame temperature, residence time) allows the synthesis of silica with specific surface areas ranging from 50 to 400 m^2/g. One aggregate consists of primary particles of nearly the same size while different aggregates generally show a size distribution of primary particles. A transmission electron micrograph is exemplarily shown in Fig. 2. On the surface of the silica particles approximately every second Si atom possesses a hydroxyl group (Si-O-H) which is termed silanol group. Depending on the *p*H, suspensions of pyrogenic silica exhibit different stability properties. At a *p*H around 2 stability results from steric repulsion of attached layers of water molecules. At *p*H values above 9 an increased number of $Si\text{-}O^-$ groups leads to a counterionic stabilization due to repulsive forces induced by the overlapping dielectric double layers [5]. According to Iler [22] and Knoblich and Gerber [31] at a *p*H around six silica suspensions are most likely to perform a phase transition.

The studied silica grades were supplied by Wacker-Chemie AG, Burghausen, Germany as dry powder. An extensive dispersion was necessary to obtain a reproducible state of the suspensions. First, the required mass of the silica powder was dispersed in an aqueous solution of potassium nitrate while stirring the liquid (if necessary by utilization of a rotor-stator disperser). Afterwards, the suspension was stirred for 30 min followed by a 10 min agitation with a rotor-stator disperser (Ultra-Turrax T50, IKA, Germany). The process was finished by a 4 min sonification with a 2/2 s on/off pulse (600 W, VibraCell VCX600, Sonics & Materials, Inc., USA). The progress of dispersion was monitored using laser diffraction (HELOS 12 KA/LA, Sympatec GmbH, Germany) after each step. Between these process steps the suspension was cooled. Afterwards, the *p*H of the sample was adjusted to 6 with potassium hydroxide. Table II shows the prepared samples. After the experiment the weight fractions of the samples were determined via a halogen moisture balance (HG53, Mettler-Toledo, Germany).

TABLE II. Survey of the prepared samples of silica suspensions.

Mass fraction [wt. %]	Specific surface area [m^2/g] (BET)	Ionic strength [M] (KNO_3)
11.0	50	0.1
10.8	100	0.1
10.0	100	0.03
13.4	150	0.1
10.7	150	0.1
9.9	150	0.03
10.1	300	0.03

B. Methods

For the DLS measurements a Malvern HPPS (Malvern Instruments Inc., UK) was used. A helium-neon-gas laser generates a vertically polarized beam of 632.8 nm wavelength in vacuum. The scattered light is detected at an angle of 173° in the backscattering regime. Here, multiple scattering is much less pronounced due to the fact that the decay rates of single and double scattering are equal so that only multiple scattering of order ≥ 3 gives rise to faster decays of the correlation function [32]. Additionally, the path lengths that a photon has to travel in the suspension are much shorter than in classical DLS setups.

All measurements were performed at a temperature of 25 °C using multiple runs under the assumption that the state of the dispersion did not change during one run. The total correlation time of one run was increased from 90 to 1800 s with the waiting time to ensure statistical confidence of the long-time correlation signals.

Additionally to DLS we used a light transmission technique to investigate the phase transitions in a larger measurement volume than with DLS. The physics behind is the dependency of the scattered light intensity on the evolving structure [6]. A decrease of the intensity should indicate a glass formation (decrease of osmotic compressibility) while an increase has to be expected for a gelation (growing clusters). For gels this statement is based on the earlier work of Nicolai and Cocard [21] who worked at angles of 25° to

145°. In this case, the increase in the scattered intensities due to gelation decreased with increasing angle. For the large scattering angle of 173° employed here, valid information is not available.

Transmission measurements were conducted with the Aello 1400 (Aello c/o GWT TU Dresden GmbH, Germany), that is a plug-in sensor able to detect the dynamic and spectral extinction of light (DES). In every run the transmitted light intensities at three different wavelengths [red 670 nm (laser), blue 470 nm, and infrared 875 nm (LED)] and the temperature are measured. The transmission of light through the sample can be determined from the intensity ratio of the sample containing the scatterers and the pure suspension medium. The measurable particle size range lies approximately between 0.06 and 250 μm. This indicates that the size of the laponite particles is too small to be detected. This was confirmed in test runs so DES could only be used as an additional tool for the pyrogenic silica samples. As the extinction of the light beam in the sample due to scattering events is measured, the results of DES should be just the opposite to the predicted behavior of scattered light by Tanaka *et al.* [6] since $I_{\text{transmission}}=I_0-\Sigma I_{\text{scattering}}$; i.e., the transmission should increase during a glass formation and decrease during a gelation. Prior to every measurement the sensor was calibrated with an aqueous solution with the same ionic strength as the sample to be measured. The samples were placed in a water bath with a temperature of 25 °C. The individual measurements were performed every 10 min until the transmission did not change anymore.

IV. RESULTS AND DISCUSSION

The typical evolution of the ACFs during a phase transition is presented in Fig. 3. All measurements are displayed until the intercept value of the ACF drops significantly (which is the first unambiguous sign of the ergodic to nonergodic transition). All laponite samples show a distinct stretching at long decay times [2,3]. In principle, the evolution of the measured ACFs for pyrogenic silica looks similar to the clay sample (see Fig. 4). However, from these pictures the evolving structure cannot be deduced.

Qualitatively, the calculated correlation functions of the fluctuating field (CFF) show the same behavior as the ACFs. The advantage in only processing the ergodic part of the correlation function [Eq. (8)] is expressed in slightly larger free diffusing portions in the sample [first term in Eq. (8)]. The exponential decay times are changed accordingly. Additionally, the stretching at the long-time tail of the CFF is lower compared to the ACF. This shows that due to partly nonergodic contributions the ACF is not suitable for diffusivity analysis. Therefore, we will proceed the whole analysis of the measured data with the CFFs to ensure that only ergodic contributions are present. The ACF data will also be given for comparison with, e.g., other publications.

A. Laponite

The phase transition times as obtained by the analysis of the measured data by Eqs. (8)–(10) of the laponite samples

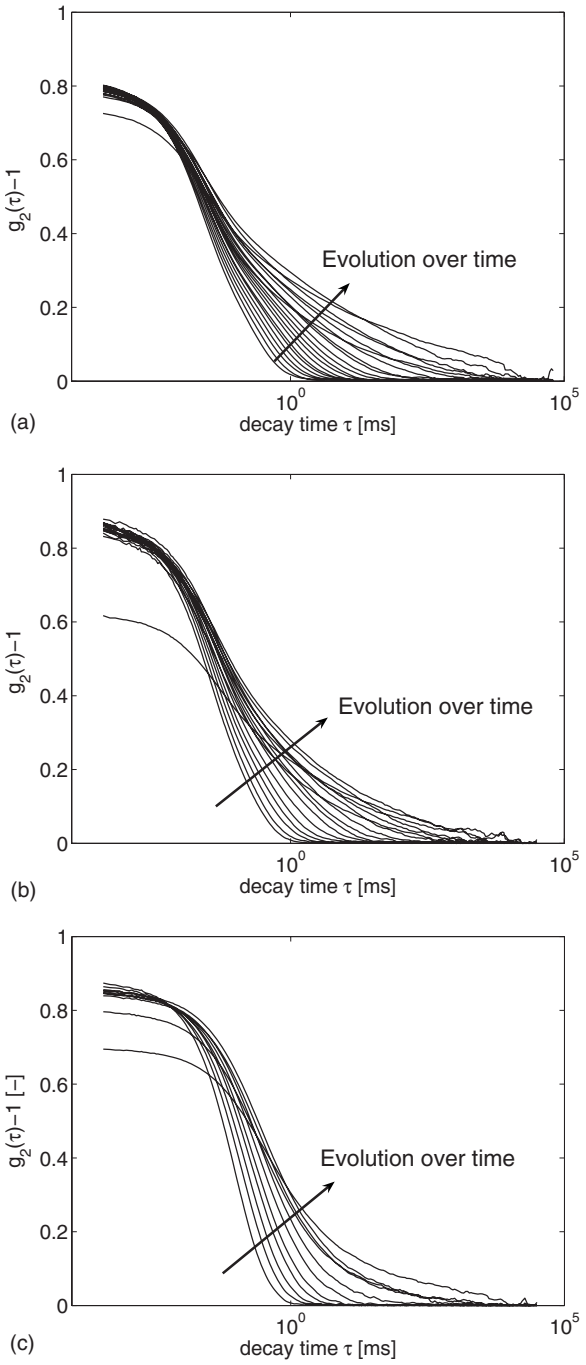

FIG. 3. Typical progressions of autocorrelation functions measured at laponite samples with (a) 2.82 wt. %, $C_S=0$ M, time span: 10:11 h, (b) 2.29 wt. %, $C_S=4\times10^{-4}$ M, time span: 11:44 h, and (c) 1.00 wt. %, $C_S=5\times10^{-3}$ M, time span: 7:17 h.

are presented in Table III. Again, the first obvious result is that always the phase transition time computed using the ACF is shorter than t_{PT} from the CFF. Thus, an erroneous consideration of the static intensity I_c results virtually in a faster solidification.

Generally, an increase in solids fraction and ion concentration leads to a faster phase transition. This can be attributed to two different scenarios. First, as proposed by Tanaka [6,19] a change in the evolving structure might cause this

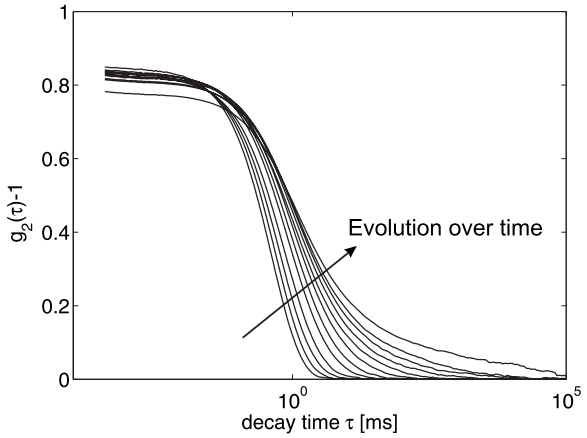

FIG. 4. Typical progression of the autocorrelation functions measured at pyrogenic silica samples; pyrogenic silica S_m =150 m^2/g, 9.9 wt. %, C_S=0.03 M, time span: 42 h.

difference as a glass formation is slower than a gelation. Secondly, if we do not neglect aggregation of the primary laponite particles at all [4], we may also use the two step model proposed by Sandkühler *et al.* [17] and examine the influence of solids fraction and electrolyte concentration on the aggregation and interconnection steps. Clearly, the velocity of the interconnection step must depend on the available interconnection points on the laponite particles and their screening. These clearly scale with solids fraction of the laponite particles. The screening of the interconnection points depends on the ionic strength of the suspension. An increase here reduces the dielectric double layer around the particles and eases the aggregation of particles and the interconnection. The question of which effect (aggregation or a different phase transition) is predominant in the specific sample is difficult to identify.

The phase transition kinetics may provide more insight into the progress of the solidification. Therefore, the mean decay time τ_{mean} is plotted over the normalized waiting time t/t_{PT} in Fig. 5(a). Here we find two different kinetic regimes (marked as groups I and II in the diagrams) which accord with the previous results of Ruzicka *et al.* [3]. The same observation can be made for τ_2 [Fig. 5(b)]. For β [Fig. 5(c)] different kinetics types can be distinguished as well, but the classification is not as sharp for the sample with high ionic strength as for, e.g., τ_2. Ruzicka *et al.* [3] investigated samples of laponite with C_S=0 M at different concentrations and found a transient range at 1.5–1.8 wt. %. Here, the transient range at C_S=0 M was found at slightly higher concentrations between 1.96–2.24 wt. %. However, the classification of the two groups also holds for higher electrolyte concentrations though the transient range seems to be shifted to lower concentrations with increasing ionic strength.

TABLE III. Phase transition times for the laponite samples computed from the ACF and CFF, respectively.

sample		phase transition time (t_{PT}) [h]	
wt. %	C_S [M]	ACF	CFF
2.82	0	16.4	20.1
2.24	0	43.1	51.7
1.96	0	84.1	87.6
1.29	0	404.2	417.8
2.29	4×10^{-4}	16.5	18.4
1.9	4×10^{-4}	21.8	22.6
1.0	5×10^{-3}	12.7	14.2

Some questions have to be raised in connection with these results. The first one is whether the solids content is truly the main influencing parameter on the kinetic regimes. Secondly, is there a certain electrolyte concentration where no available solids content produces a kinetic regime of group II (transient concentration $\rightarrow$0)?

As it was not the goal of our investigations to fully explain the kinetics of laponite phase transitions we restrict our interpretation on the two measured regimes. Ruzicka *et al.* [3] explain the two different kinetic regimes at low ionic strength by the formation of Wigner glasses from single laponite platelets at high solids content and by aggregated laponite particles at low concentrations. Again, the aggregation step seems to control the speed of the phase transition. According to Sandkühler *et al.* [17] the interconnection step is faster by far than the aggregation. This may also be associated with an entrapment step in the formation of a Wigner glass. In view of this theoretical interpretation our results can also be explained. As mentioned above a higher electrolyte content speeds up the aggregation process by a screening of the electrostatic repulsion forces which leads to a faster aggregation [12,20]. Additionally, faster aggregation produces more irregular aggregate structures with a higher porosity. Thus, the second step (interconnection or entrapment) may start earlier and we get a relatively faster phase transition already at lower solids fractions.

The increase of the fit parameter τ_1 [see Fig. 5(d)] supports the assumption that we indeed have an aggregation of laponite particles as it describes the remaining freely diffusing portions of the measured spectra. The same has been measured by Ruzicka *et al.* [3]. They found a dependence of the steepness of the increase with decreasing solids fraction which cannot be found in our experiments. However, it can be noticed that at C_S=0 M and the lowest measured solids fraction the increase is monotonic while by increasing the solids fraction a maximum with a following decrease of τ_1 can be observed. An explanation can be that at first laponite particles aggregate but get entrapped later so that the contribution of rotational diffusion becomes more important in the measurement signal. Since the decay times of rotational diffusion are lower than for translational diffusion [24] this leads to a drop of τ_1. This effect is especially enhanced at large scattering angles [33] so it might not be observable with a standard DLS device as used in the experiments of Ruzicka *et al.* [3].

An increase in the ionic strength of the suspensions leads to a shift of the τ_1 curves to larger values; i.e., seemingly we first get a fast aggregation due to the screened Coulomb forces followed by a slow aggregation. For $C_S=4\times10^{-4}$ M we again observe a transition from monotonic increase of τ_1 to a maximum with following decrease with increasing volume fraction. The transition concentration is thereby slightly

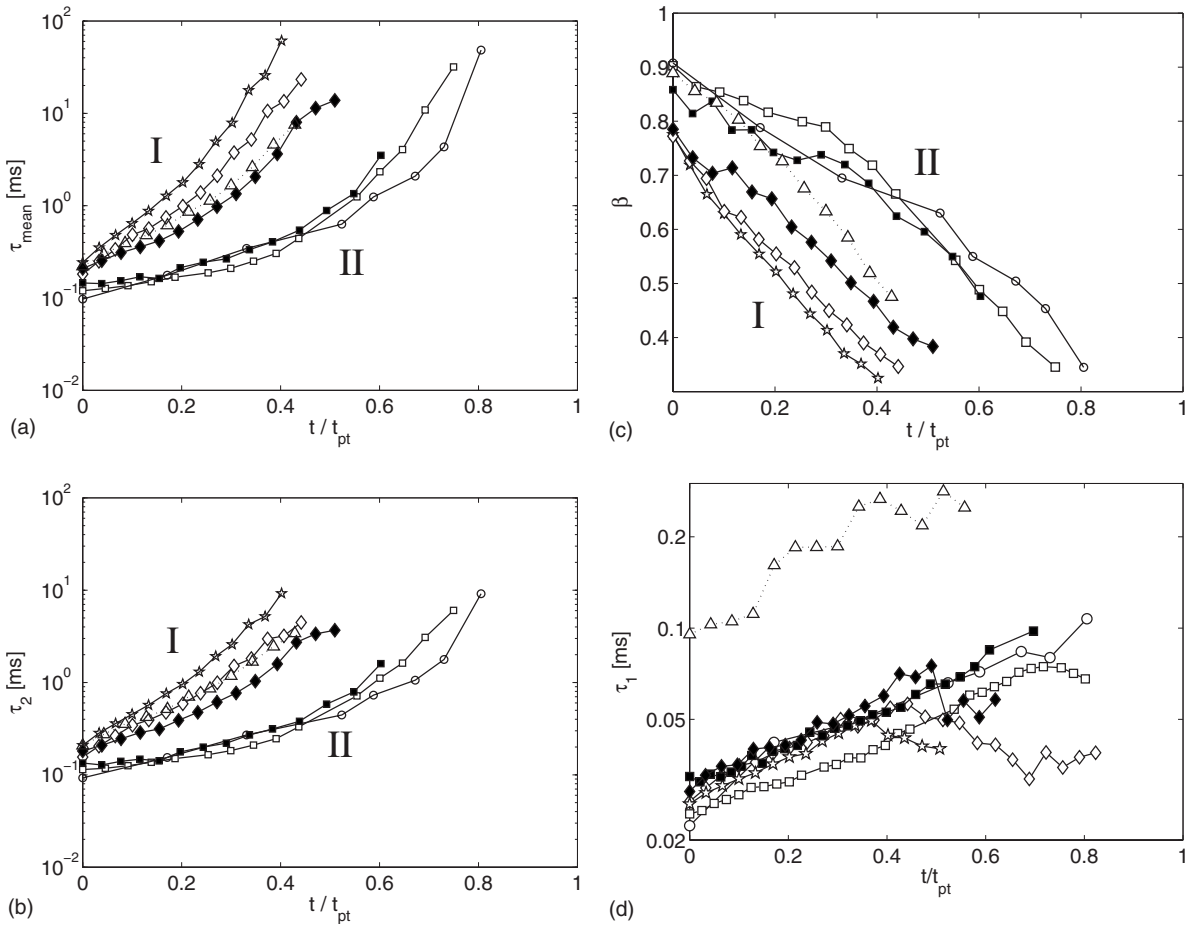

FIG. 5. Calculated data from the CFF of the laponite samples, x axis normalized with the computed phase transition time; C_S=0 M, open stars: 2.82 wt. %, open diamonds: 2.24 wt. %, open squares: 1.96 wt. %, open circles: 1.29 wt. %; $C_S=4\times10^{-4}$ M, filled diamonds: 2.29 wt. %, filled squares: 1.9 wt. %; $C_S=5\times10^{-3}$ M, 1.00 wt. % dotted line with triangles, groups marked with I and II in the diagrams.

increased, suggesting that aggregation is a more important step at higher ionic strength.

Summarizing we can say that in our measurements we indeed find aggregation of laponite particles for all ionic strengths and solids fractions but it is not possible to identify the evolving final structure of the arrested phase from the transition kinetics. Tanaka *et al.* [6] suggest the scattered light intensity to be an additional clue to identify the evolving structure. Therefore, we used the recorded mean count rate of each single DLS measurement run as an equivalent to observe the scattered light intensity. Figure 6 shows two examples for the kinetics groups I and II, respectively. The remaining samples show the same principal behavior. Close to the phase transition time, the scattered light intensity of the samples shows rapid changes and no continuous evolution. These are due to the arising nonergodicity of the sample; a mean value would only be measurable from position-dependent measurements. But, at least up to t/t_{PT} =0.5, there is a measurable difference in the evolution of the scattered light intensities between the two groups. Unfortunately, as both groups do not show a monotonic behavior, we cannot compare our results with the predictions of Tanaka *et al.* [6] who expect a monotonic decrease for a glass transition and an increase for a gelation. This different behavior might be due to the large scattering angle where no previous measurements of phase transitions are known to the authors. Finally, clear evidence on the structure of the arrested phases

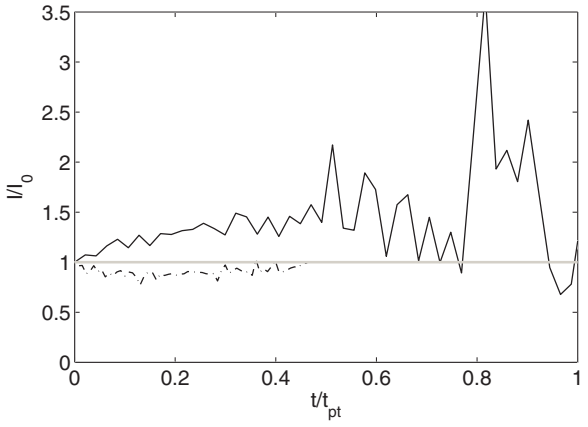

FIG. 6. Measured scattered light intensities at 173° determined from the DLS experiments, normalized to initial intensity over relative phase transition time; solid line: laponite 1.00 wt. %, C_S=5 $\times10^{-3}$ M (group I); dashed line: laponite 1.96 wt. %, C_S=0 M (group II).

TABLE IV. Calculated phase transition times from the ACF and CFF of the pyrogenic silica samples.

Sample			Phase transition time (t_{PT}) [h]	
BET [m^2/g]	wt. %	C_S [M]	ACF	CFF
50	11.0	0.1	22.4	23.6
100	10.8	0.1	22.7	24.7
100	10.0	0.03	116.5	136.8
150	13.4	0.1	2.8	3.0
150	10.7	0.1	3.3	3.3
150	9.9	0.03	49.0	50.4
300	10.1	0.03	5.3	5.6

of our laponite samples cannot be drawn. However, we have obtained the same kinetics regimes that have been measured by Ruzicka *et al.* [3] and an aggregation of the laponite particles is observable. Thus, we now have a reliable experimental methodology to transfer these results to another material system.

B. Pyrogenic silica

The data of the pyrogenic silica suspensions were analyzed in exactly the same manner as those of the laponite samples. All samples revealed a fluid-solid phase transition in time periods ranging from 3 h to 5 days. When weak ultra sound of 50 W was applied to the solidified samples in a water bath only those of low ionic strength could be redispersed. This shows that the interparticle interaction strength increases with ionic strength. Table IV presents the calculated phase transition times from both the ACF and the CFF of the suspensions. Again t_{PT} is lower for the ACF.

Generally, an increase of the specific surface area and the ionic strength, respectively, leads to a faster phase transition with the exception of the samples with 50 and 100 m^2/g specific surface area at $C_S=0.1$ M. An increase in the solids concentration also speeds up the solidification as shown for the two samples with 150 m^2/g. We can again use the model of Sandkühler *et al.* [17] to explain these effects. An increase in solids fraction and specific surface area, respectively, increases the available interconnection points on the particles which in turn is relevant for the velocity of the phase transition. As the interconnection step is faster than the aggregation step, this influence is lower than a screening of the Coulomb forces by an increase of the ionic strength which drastically reduces the phase transition times. This can, e.g., be seen for the samples with constant specific surface area and constant solids content. This behavior is also similar to laponite suspensions where adding salt to the solutions speeds up the aggregation of the particles.

The analysis of the phase transition kinetics in Fig. 7 also shows a classification into two groups for τ_{mean} and τ_2 as was the case for the laponite samples. On first sight this suggests a universal behavior of colloidal solid-liquid phase transitions. However, the classification is not obtained for the stretching parameter β. Here, the curves indicate a dependence on the specific surface area and the ionic strength of the suspensions but the data basis is not sufficient for a detailed analysis. The thick solid line in Fig. 7(c) visualizes a result obtained from laponite (1.00 wt. %, $C_S=5\times10^{-3}$ M). As we obtain nearly the same evolution and final values for the pyrogenic silica samples, we may conclude that similar mechanisms lead to the phase transition in both systems. The strong variations at $t/t_{PT}<0.2$ are due to the fit equation [Eq. (8)]. For a beginning phase transition β takes values around 1; i.e., the CFF is not stretched yet. The two decays in the fit may then represent nearly the same section in the correlation function and, therefore, the algorithm has four variables (τ_1, τ_2, β, and a) to minimize the residual. Thereby, the influence of measurement errors is strongly enhanced, which leads to the observed variations.

No classification is also obtained for the parameter τ_1. Similarly to the laponite suspension we see an increase of τ_1 for all measured samples which indicates aggregation. The curves are shifted on the y axis with decreasing specific surface area at constant ionic strength which shows different sizes of the pyrogenic silica aggregates in the grades. An increase of ionic strength again leads to a fast aggregation (higher values of τ_1 at $t/t_{PT}\rightarrow0$) as was the case for laponite. This again suggests a similarity of the phase transitions in the two materials.

The significance of the three parameters, solids content, specific surface area, and ionic strength, on the phase transition kinetics [Figs. 7(a) and 7(b)] cannot be easily distinguished. However, some indications can be given. As the two samples with $S_m=150$ m^2/g and $C_S=0.1$ M that are identical except for their solids content show nearly identical phase transition times but different kinetics the solids content seems to play an important role. We obtain a transient regime that determines the shift between the two kinetics similar to laponite suspensions. Further investigations on the exact influence of solids concentration are desirable but are hampered by extremely long phase transition times superposed with a consolidation of the solid phase at lower concentrations and multiple scattering that cannot be fully suppressed by a backscattering measurement at higher concentrations.

The ionic strength seems to be another fundamental parameter on the transition kinetics. All samples with $C_S=0.03$ M can be found in kinetic group II. Due to the stronger repulsion of the aggregates at lower salt content, the aggregation process is hindered which leads to a relatively slower phase transition. The specific surface area does not have such a clear impact on the transition kinetics and only influences the total phase transition time. Summarizing, the main parameters that influence the phase transition of pyrogenic silica could be clearly identified and their impacts characterized; however, the formation of two kinetic groups and the evolving arrested structures remain to be explained by further experiments.

If we further take the measured scattered light intensities into consideration (Fig. 8) we first discover a difference between laponite and pyrogenic silica (see Fig. 6). For both kinetic groups the measured scattered light intensity drops to a plateau at about $I/I_0=0.8$ and shows strong variations for $t/t_{PT}>0.5$. As explained above we cannot conclude from this single value an evolving structure of the arrested phase since there are no values for comparison in the backscatter area.

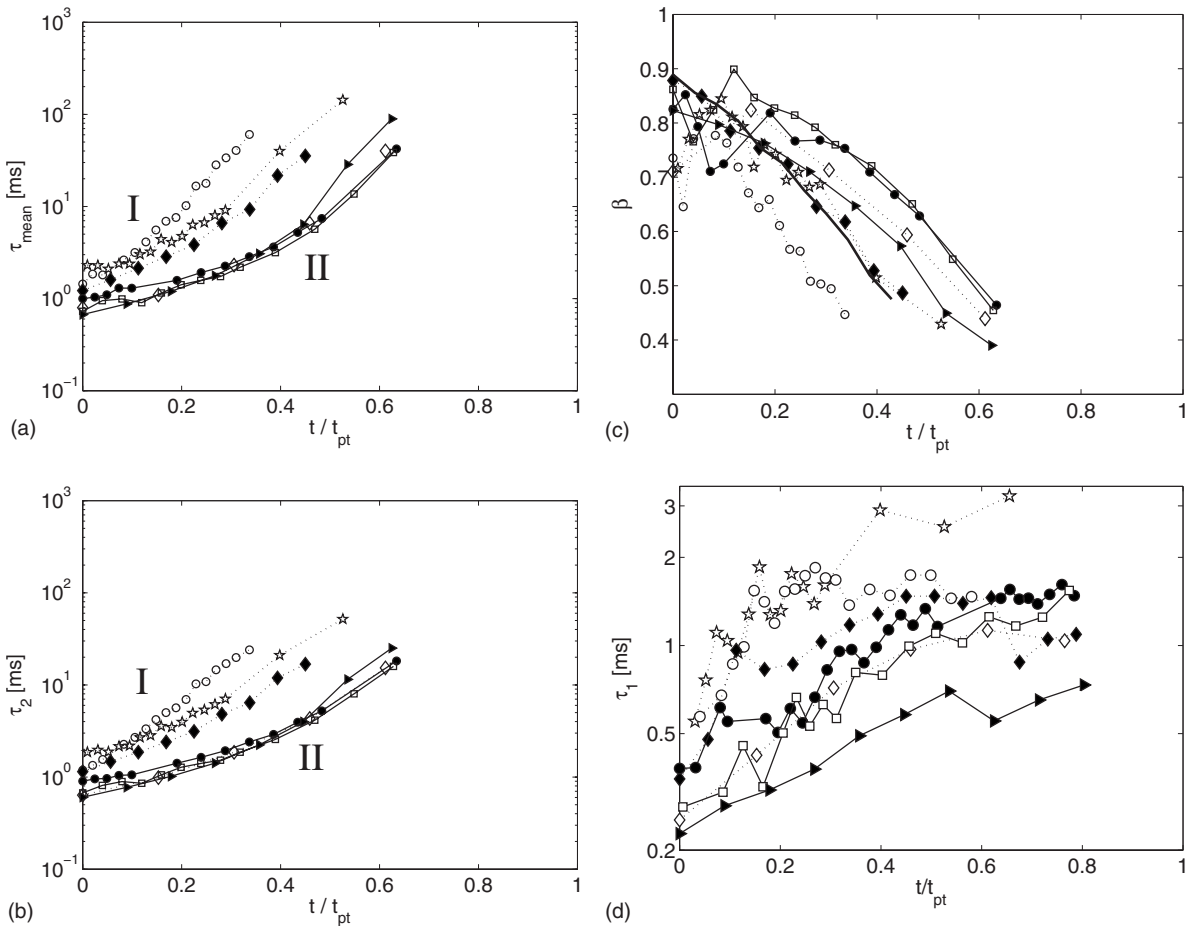

FIG. 7. Calculated data from the CFF of the pyrogenic silica samples, x axis normalized with the computed phase transition time; dashed lines: C_S=0.1 M, stars: 50 m^2/g, 11 wt. %, open circles: 100 m^2/g, 10.8 wt. %, filled diamonds: 150 m^2/g, 13.4 wt. %, open diamonds: 150 m^2/g, 10.7 wt. %; thin solid lines: C_S=0.03 M, filled circles: 100 m^2/g, 10 wt. %, squares: 150 m^2/g, 9.9 wt. %, filled triangles: 300 m^2/g, 10.1 wt. %; thick solid line in (c): laponite 1 wt. %, $C_S=5\times10^{-3}$ M.

Therefore, for pyrogenic silica we can refer to the sum effect of all scattering events by measuring the transmission through a sample of known thickness. Figure 9(a) shows the raw transmission data of the three wavelengths of the DES measurements exemplarily for a pyrogenic silica with 300 m^2/g specific surface area, 10.1 wt. %, and C_S =0.03 M. We see a decrease of transmission for all examined wavelengths which is in contradiction to the scattered light intensity measurements at 173°. Since the transmission drops, scattering must be enhanced (if we neglect absorption inside the particles which is not present in pyrogenic silica). This shows that the measurement of a scattering signal at a single scattering angle is not sufficient to draw conclusions on the structural evolution in the sample. From the sum transmission signal we can conclude that the overall scattering at all possible scattering angles is enhanced which may be due to growing clusters of pyrogenic silica aggregates. Thus, the measurement results are a good indication that aggregation is present in the samples. However, it cannot be stated whether in the arrested phase the clusters are interconnected (which should be a gel phase) or entrapped in cages (which would be a Wigner glass).

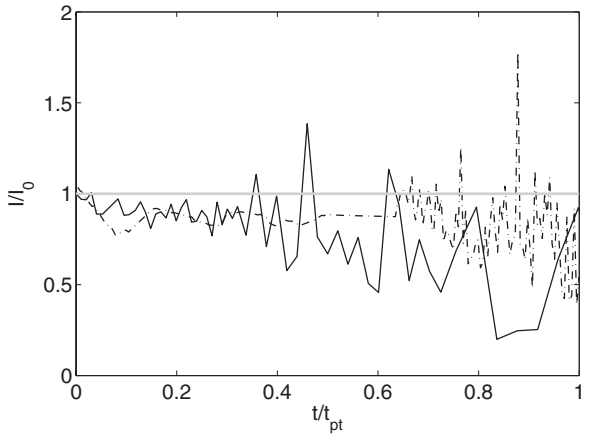

FIG. 8. Measured scattered light intensities at 173° determined from the DLS experiments, normalized to initial intensity over relative phase transition time; solid line: pyrogenic silica 100 m^2/g, 10.8 wt. %, C_S=0.1 M (group I); dash-dotted line: pyrogenic silica 100 m^2/g, 10.0 wt. %, C_S=0.03 M (group II).

Normalization of the transmission curves with $(T-T_\infty)/(T_0-T_\infty)$ results in a very similar behavior at all wavelengths [see Fig. 9(b)]. This behavior can be observed for all

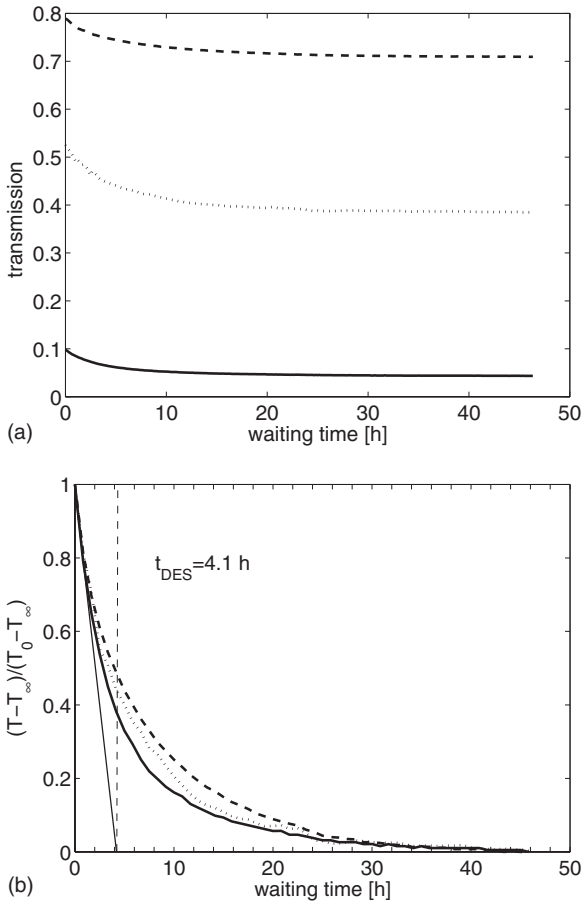

FIG. 9. Dynamic extinction spectroscopy (DES) results for pyrogenic silica suspensions, exemplarily shown for S_m=300 m^2/g, 10.1 wt. %, C_S=0.03 M; solid line: 470 nm, dotted line: 670 nm, dashed line: 875 nm wavelength.

measured pyrogenic silica samples. Especially the slope at $t=0$ is identical. Therefore, we can determine a decay time of the transmission drop by extrapolating the initial slope to $(T-T_\infty)/(T_0-T_\infty)=0$ [see Fig. 9(b)]. The procedure is similar to the determination of time constants of delays in electronics. The results of this extrapolation are displayed in Table V. The values show the same tendency as the phase transition

TABLE V. Calculated transmission decay times from the transmission data of the pyrogenic silica suspensions by dynamic extinction spectroscopy (DES).

BET [m^2/g]	sample wt. %	C_S [M]	transmission decay time (t_{DES}) [h]
50	11.0	0.1	6.6
100	10.8	0.1	7.2
100	10.0	0.03	26.9
150	10.7	0.1	3.3
150	9.9	0.03	18.8
300	10.1	0.03	4.1

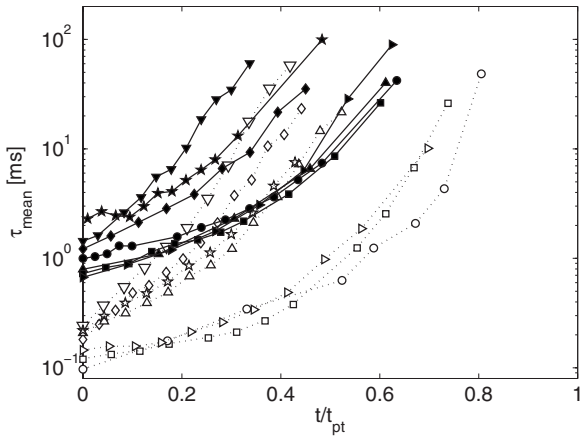

FIG. 10. Mean decay times of the fluctuating part of the scattered light intensity (CFF) for both systems in comparison; solid lines and filled symbols: pyrogenic silica: C_S=0.1 M: stars: 50 m^2/g, 11 wt. %, downward-pointing triangles: 100 m^2/g, 10.8 wt. %, diamonds: 150 m^2/g, 13.4 wt. %, upward-pointing triangles: 150 m^2/g, 10.7 wt. %; C_S=0.03 M: circles: 100 m^2/g, 10 wt. %, squares: 150 m^2/g, 9.9 wt. %, right-pointing triangles: 300 m^2/g, 10.1 wt. %; dotted lines and open symbols: laponite: C_S=0 M: downward-pointing triangles: 2.82 wt. %, diamonds: 2.24 wt. %, squares: 1.96 wt. %, circles: 1.29 wt. %; $C_S=4\times10^{-4}$ M: upward-pointing triangles: 2.29 wt. %, right-pointing triangles: 1.9 wt. %; $C_S=5\times10^{-3}$ M: stars: 1.00 wt. %.

times determined with DLS (see Table IV). They are mostly shorter (20–40 % of t_{PT}) for slow phase transition but become closer for very fast phase transitions.

This difference may be explicable with the measurement zone under consideration which is very small in a DLS experiment ($\approx10^{-6}$ cm^3) and much larger in DES ($\approx10^{-2}-10^{-1}$ cm^3). Thus, DLS measures a micromobility rather than a macromobility of the sample. The mobility measured with DES should therefore be closer to rheology results that exist, e.g., for laponite [19]. The difference between t_{DES} and t_{PT} can now be interpreted as follows: For a slow phase transition the macromobility is firstly stronger reduced than the micromobility. However, small changes of the macromobility are still possible when the micromobility in the specific measurement volume of DLS has already come to an arrest. This is reflected in the long time that is needed for the transmission signals to reach a quasifinal state. Thus, DES is a valuable tool to observe phase transition processes nonintrusive and on a larger scale than it is possible with a DLS measurement. Additionally, it has the advantage of measuring the sum of all scattering events in one signal. Of course the resolution of, e.g., a static light scattering (SLS) experiment is lost.

C. Comparison

Finally, we want to directly compare the phase transitions of pyrogenic silica and laponite. Therefore, in Fig. 10 the kinetics of τ_{mean} are plotted for both material systems. It is remarkable that both show a differentiation into two groups and additionally the two groups show a very similar behavior. The shift in the ordinate has to be attributed to the dif-

ferent sizes of laponite [approximately 15 nm when analyzed by DLS (173°) in a sol] and the silica particles (ranging from 150 to 320 nm depending on the specific surface area). This supports the assumption of a universal character of phase transitions even with completely different colloidal systems.

The principal influencing factors on the transition kinetics are the same for laponite and pyrogenic silica, the solids content and the ionic strength. Further investigations have to be conducted to finally reveal the origin of the two different kinetic regimes. Our results also suggest that different final structures evolve in the two groups. We could only show that aggregation is present in both material systems but the final step (interconnection or entrapment) could not be identified.

V. SUMMARY

Phase transitions of pyrogenic silica suspensions were examined in comparison to model laponite by DLS and DES measurements to obtain a first impression on the comparability of the two material systems in terms of their transition kinetics and influencing parameters. To overcome difficulties arising from multiple scattering contributions in classical light scattering experiments DLS equipment working in the backscattering regime was used to obtain the intensity correlation function.

The measured scattered light intensity was then decomposed into a position-independent fluctuating part and a static part that is due to nonergodic contributions to the measurement signal [2]. With this decomposition the time span in the solidifying samples could be expanded to obtain more accurate information on the transition kinetics. It was shown that the analysis of the ACF already contains nonergodic contributions at short waiting times when the intercept is still at the same level as for ergodic samples. These contributions lead to deviations in the data analysis; i.e., the phase transition times are underestimated. Consequently, all experiments were analyzed on the basis of the correlation function of the fluctuating field (CFF) to obtain the transition kinetics.

For the laponite suspensions we obtained phase transition kinetics that split up into two groups. This is in accordance with the results of Ruzicka *et al.* [3,34]. This uniform character of the phase transitions does not generally correspond to the ionic strength of the suspensions but on the solids content.

Phase transitions of pyrogenic silica suspensions were first examined using DLS techniques. The analysis of the CFF also shows two groups of phase transition kinetics. In their principal evolution the transitions look very similar to the laponite samples, thus suggesting a universal character of phase transitions. The specific surface area could be identified as an important parameter that controls the phase transition time but its influence on the transition kinetic could not be clarified. Solids concentration also has an important effect on the kinetic regime. It should therefore be subject to further investigations. An increase of the ionic strength also speeds up the phase transition as was the case for the laponite samples, so the main influencing parameters are the same for both materials.

Finally, we have shown that dynamic extinction spectroscopy is a valuable tool for the characterization of phase transitions on a macroscale due to the multiwavelength and nonintrusive measurement. The determined transmission decay time may also be used to classify different phase transitions. However, at least slightly turbid samples are required for a good data quality.

ACKNOWLEDGMENT

The authors wish to thank Wacker-Chemie AG, Burghausen, Germany, for the financial support of this study.

APPENDIX: CALCULATION OF THE CFF FROM MEASURED AUTOCORRELATION DATA ACCORDING TO REF. [2]

At the particular time $t=0$ the ACF reduces to

$$g_2(0) = \frac{\langle I(t)^2 \rangle}{\langle I(t) \rangle^2}. \tag{A1}$$

The mean count rate $\bar{I}$, which is conform with $\sqrt{\langle I(t) \rangle^2}$, is another parameter of the measurement system. Hence we obtain for Eq. (4):

$$I_c = \sqrt{2\langle I(t) \rangle^2 - g_2(0)\langle I(t) \rangle^2} = \bar{I}\sqrt{2 - g_2(0)}. \tag{A2}$$

I_c vanishes for a perfect correlation when $g_2(0)=2$. $\langle I_f(t) \rangle$ then can be substituted with the help of Eqs. (A3) and (A2):

$$\frac{\langle I_f(t) \rangle}{\langle I(t) \rangle} = \frac{\langle I(t) \rangle - I_c}{\langle I(t) \rangle} = 1 - \sqrt{2 - g_2(0)}. \tag{A3}$$

Applied to Eq. (5) we obtain the following relation for the CFF:

$$h(\tau) = 1 + [1 - \sqrt{2 - g_2(0)}]^{-1}\{\sqrt{g_2(\tau) - g_2(0) + 1} - 1\}. \tag{A4}$$

[1] R. J. Hunter, *Foundations of Colloid Science* (Clarendon Press, Oxford, 1993), Vol. 1.

[2] M. Kroon, G. H. Wegdam, and R. Sprik, Phys. Rev. E **54**, 6541 (1996).

[3] B. Ruzicka, L. Zulian, and G. Ruocco, J. Phys.: Condens. Matter **16**, S4993 (2004).

[4] P. Mongondry, J. F. Tassin, and T. Nicolai, J. Colloid Interface Sci. **283**, 397 (2005).

[5] B. P. Binks and S. O. Lumsdon, Phys. Chem. Chem. Phys. **1**, 3007 (1999).

[6] H. Tanaka, J. Meunier, and D. Bonn, Phys. Rev. E **69**, 031404 (2004).

[7] P. N. Pusey and W. van Megen, Phys. Rev. Lett. **59**, 2083 (1987).
[8] W. van Megen and S. M. Underwood, Phys. Rev. E **49**, 4206 (1994).
[9] T. Eckert and E. Bartsch, Phys. Rev. Lett. **89**, 125701 (2002).
[10] K. A. Dawson, Curr. Opin. Colloid Interface Sci. **7**, 218 (2002).
[11] A. Coniglio, L. de Arcangelis, E. del Gado, A. Fierro, and N. Sator, J. Phys.: Condens. Matter **16**, S4831 (2004).
[12] F. Sciortino, S. Mossa, E. Zaccarelli, and P. Tartaglia, Phys. Rev. Lett. **93**, 055701 (2004).
[13] Y. Kantor and T. A. Witten, J. Phys. (France) Lett. **45**, L675 (1984).
[14] S. Manley, H. M. Wyss, K. Miyazaki, J. C. Conrad, V. Trappe, L. J. Kaufman, D. R. Reichman, and D. A. Weitz, Phys. Rev. Lett. **95**, 238302 (2005).
[15] P. N. Segrè, V. Prasad, A. B. Schofield, and D. A. Weitz, Phys. Rev. Lett. **86**, 6042 (2001).
[16] S. Manley *et al.*, Phys. Rev. Lett. **93**, 108302 (2004).
[17] P. Sandkühler, J. Sefcik, and M. Morbidelli, Adv. Colloid Interface Sci. **108-109**,133 (2004).
[18] R. Bandyopadhyay, D. Liang, H. Yardimci, D. A. Sessoms, M. A. Borthwick, S. G. J. Mochrie, J. L. Harden, and R. L. Leheny, Phys. Rev. Lett. **93**, 228302 (2004).
[19] H. Tanaka, S. Jabbari-Farouji, J. Meunier, and D. Bonn, Phys. Rev. E **71**, 021402 (2005).
[20] L. Li, L. Harnau, S. Rosenfeldt, and M. Ballauff, Phys. Rev. E **72**, 051504 (2005).
[21] T. Nicolai and S. Cocard, Eur. Phys. J. E **5**, 221 (2001).
[22] R. K. Iler, *The Chemistry of Silica* (Wiley Interscience, New York, 1979).
[23] R. Finsy, Adv. Colloid Interface Sci. **52**, 79 (1994).
[24] R. Xu, *Particle Characterization: Light Scattering Methods, Particle Technology Series* (Kluwer Academic, London, 2000).
[25] B. Abou, D. Bonn, and J. Meunier, Phys. Rev. E **64**, 021510 (2001).
[26] D. Szász, Stud. Sci. Math. Hung. **31**, 299 (1996).
[27] D. Bonn, H. Tanaka, G. Wegdam, H. Kellay, and J. Meunier, Europhys. Lett. **45**, 52 (1998).
[28] D. Bonn, H. Kellay, H. Tanaka, G. Wegdam, and J. Meunier, Langmuir **15**, 7534 (1999).
[29] A. Mourchid and P. Levitz, Phys. Rev. E **57**, R4887 (1998).
[30] R. Bode, H. Ferch, and H. Fratzscher, Kautsch. Gummi Kunstst. **20**, 578 (1967).
[31] B. Knoblich and T. Gerber, J. Non-Cryst. Solids **283**, 109 (2001).
[32] H. Wiese and D. Horn, J. Chem. Phys. **94**, 6429 (1991).
[33] H. M. Lindsay, R. Klein, D. A. Weitz, M. Y. Lin, and P. Meakin, Phys. Rev. A **38**, 2614 (1988).
[34] B. Ruzicka, L. Zulian, and G. Ruocco, Langmuir **22**, 1106 (2006).